

Comparison of Adsorption Properties of Different Configurations of CDI Cells

Shouguang Yao, Yunfei Zhu

Jiangsu University of Science and Technology, Zhenjiang 212100, China

*E-mail: zjyaosg@126.com

Received: 11 February 2021 / Accepted: 12 April 2021 / Published: 30 April 2021

This study aims to investigate the influence of different configurations of capacitive deionisation (CDI) cells on desalination performance. Based on the modified Donnan model, a three-dimensional transient model of a CDI desalination unit considering the coupling of solution flow, charge transport and electric field and potential was established, and the entire adsorption process was simulated. After conducting experiments to verify the accuracy of the model, four CDI units with different architectures were set first, after which the flow state of the solution in the four CDI units were compared, along with the influence on the desalination performances of the CDI units. Finally, the influences of different inlet velocities on the desalination performances of the CDI units were compared and analysed. Simulation results reveal the following: (1) if the boundary conditions are the same, compared with the plate-inflow/outflow CDI unit, the middle hole of the plate flows into the two-hole outflow CDI unit, the flow from the middle of the square plate to the surrounding outflow CDI unit and the flow from the middle of the disk to the surrounding outflow CDI unit reduced the average flow velocities of the solutions in the flow passage to 34.04%, 16.88%, and 15.96%, respectively. This also resulted in the corresponding increase in the retention time of the solution in the flow passage by 40%, 44.52%, and 50.95%, resulting in better desalination performance than that of the plate-inflow/outflow CDI unit. (2) Compared with the three other types of CDI units, the one with middle holes flowing in and out at both ends of the plate generates a 0 m/s solution flow rate at the four corners, which cannot easily flow out, thus reducing the desalination performance of the CDI unit. (3) Apart from the inlet velocity boundary condition, all other boundary conditions are the same. Thus, improving the inlet flow rate can help transform the flow around the square plate into a middle-type CDI unit, and the disc into the flow around the CDI unit can effectively reduce desalination and lessen the impact of inlet velocity increase. This can also reduce the CDI unit desalination performance of less than flat CDI unit and flow type and transform a flat-type hole into two holes in the CDI unit.

Keywords: Capacitive deionisation (CDI); MD model; fluid distribution; three-dimensional transient model; numerical simulation.

1. INTRODUCTION

At present, the intensifying fresh water crisis has affected the sustainable development of human society [1]. Thus, more and more people are paying attention to the development of sustainable and energy-efficient seawater desalination methods. Amongst these technical methods, the capacitive deionisation (CDI) technology stands out for its high-efficiency, energy-saving and environmental protection advantages [2–5].

In relation to the use of CDI, it is important to accurately simulate and explain the internal mechanism of desalination in CDI cells and to establish an appropriate multi-field coupling analysis model. Due to the irrational assumption that the classical GCS model cannot be directly applied to the CDI process [6,7], Biesheuvel further proposed the modified Donnan (MD) model and demonstrated by experiments [8–12] that the MD model can well describe the data of salt adsorption and charge storage in CDI under the influence of strongly overlapping double electric layers. Based on MD model theory, Guyes [13,14] established a one-dimensional (1D) analytical model that only considered charge transport and electric field and potential coupling. That model assumed the presence of a static solution between the electrodes and that the ion concentration in the diffusion layer away from the electrode remained constant; however, it did not consider the effect of the solution flow on ion adsorption. Following MD model theory, Hemmatifar [15] established solution flows, charge transport electric potential and electric field coupling analysis of a two-dimensional (2D) CDI model. This was achieved by studying the ions in the solution during porous plate electrode electrical migration and the diffusion of the model as well as by explaining ion migration and diffusion in porous electrode plates. However, the proposed model only considered the effect on ion adsorption of the solution flow in the middle region of the channel.

Numerous studies have focused on modelling a working cycle of CDI as a process [16–18] and on enhancing desalination performance of CDI cells by improving electrode materials [19–21] and optimising operating parameters [22–24]. In comparison, only a few studies have optimised fluid flow in CDI devices [25,26]. Laxman [27], for example, used Fluent software to build models for CDI units with different configurations. That work studied the flow velocity and pressure distribution of the solution in the model by comparing the pressure drop, fluid flow parameters and salt adsorption capacity obtained in the experiment. However, this model only considered the flow of solution in CDI units of different configurations without coupling the flow of solution with charge transport and electric field and potential. Thus, it cannot be considered a complete CDI analysis model.

Due to the lack of a complete 3D transient analysis model for CDI units and the analysis of different flow configurations, the current paper proposes a three-dimensional (3D) transient model of CDI seawater desalination unit based on the MD model. The proposed model was established whilst considering the coupling of solution flow, charge transport as well as electric field and potential. After verifying the accuracy of the model through experiments, four CDI cells with different configurations were set based on the model, and the flow state of the solution in CDI cells under these configurations were compared and studied, along with the influence on ion adsorption. This work also investigated the influence of different inlet flow rates on the desalination performances of the four CDI cells with varying configurations.

2. MODEL ESTABLISHMENT

2.1 Physical model

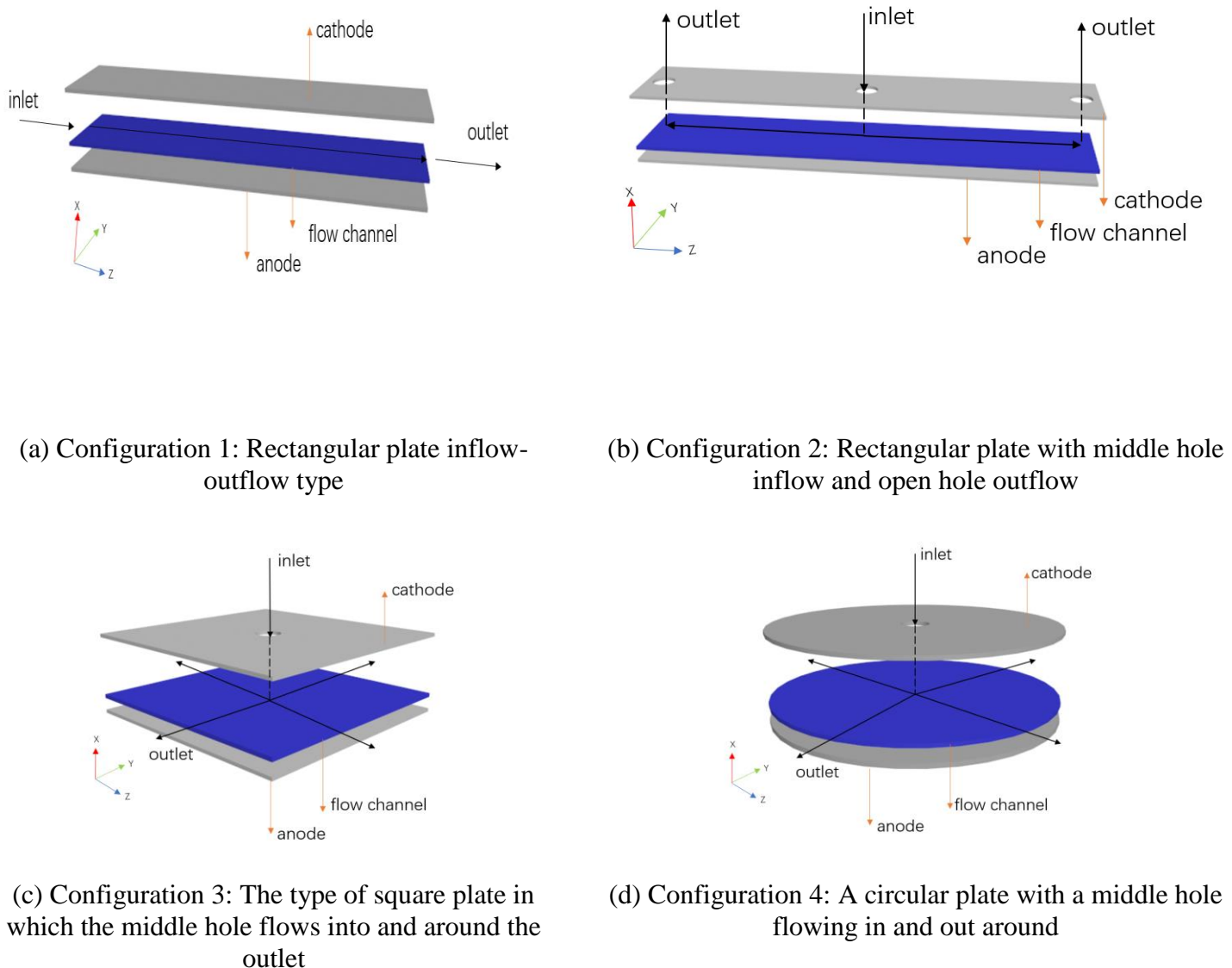


Figure 1. Physical model diagrams of four types of CDI units

Four flow configurations were set with a typical FB (Flow By) structure [28,29] CDI unit, as shown in Figure 1. These are described as follows:

Configuration 1: Rectangular plate inflow outflow type;

Configuration 2: Rectangular plate with middle hole inflow and open hole outflow;

Configuration 3: The type of square plate in which the middle hole flows into and around the outlet; and

Configuration 4: A circular plate with a middle hole flowing in and out around.

The physical model included a positive and negative porous carbon electrode and an intermediate main channel. The key geometric dimension parameters required for calculation are shown in Table 1.

For the coordinates, we defined x direction for CDI unit thickness direction, y direction for width direction and z fluid direction of the flow passage of the main flow direction. Blue represents the solution in the flow channel and grey represents the porous carbon electrode. The black arrows represent the direction of flow of the solution. According to the study on the ion adsorption and desorption process in CDI units, the following hypotheses are made [30]:

- (1) The solution is a homogeneous dilute NaCl solution, and the solute exists in the free form of monovalent anion and cation.
- (2) Flow is considered as single-phase, incompressible low-speed laminar flow, and the influence of the inlet section is ignored.
- (3) The electrode and solution in the unit are regarded as isotropic, and the physical parameters of the material are fixed.
- (4) There is no heat exchange between the research unit and the outside world, and the influence of gravity is ignored;
- (5) The non-electrostatic adsorption force in the porous electrode is constant and has a value of 1.5.

The setting of the physical model parameters of the proposed CDI unit is shown in Table 1.

Table 1. Parameter settings of the proposed CDI unit model [15]

Parameter	Unit	Value	Description
L	mm	100	Length of flat plate
W	mm	20	Plate width
L_e	mm	0.68	Plate thickness
L_s	mm	0.8	Gap thickness
L_{square}	mm	44.7	Square plate electrode length
R	mm	25.3	Disc-shaped electrode radius
r	mm	2.5	Inlet/outlet hole radius
P		0.7	Plate porosity
μ_{att}		1.5	Non-electrostatic adsorption parameter
D_{Na}	m^2/s	0.95×10^{-9}	NaCl solution Na^+ ion diffusion coefficient
D_{Cl}	m^2/s	0.95×10^{-9}	NaCl solution Cl^- ion diffusion coefficient
c_{in}	mol/m^3	100	Inlet concentration of NaCl solution
u_{in}	m/s	0.025	Inlet flow rate of NaCl solution

2.2 Model establishment

2.2.1 MD model

The MD model considers the influence of the overlapping double electrical layers in the porous electrode. Thus, it can more accurately describe the adsorption/desorption of the CDI cell using porous material as the electrode. For this reason, the MD model is used for description and analysis. Here, we use the bimodal pore structure for porous electrode to distinguish the big holes (diameter greater than or

equal to 50 nm) from the smaller holes (less than 2 nm in diameter) (microporous subscript m, macroporous subscript m and channel subscript). The ion transport takes place in the interconnected macropores inside the porous electrode, and the pore region is occupied by the double electric layer [8,31–32]. When chemical equilibrium is reached, there is no electrochemical potential gradient between the micropores and macropores. Therefore, an extended Boltzmann distribution can be used to correlate the micropore and macropore concentrations of ions [33]

$$C_{m,i} = C_{M,i} \cdot \exp\left(-Z_i \frac{\Delta\phi_D}{V_T} + \overline{\mu}_{att}\right), \quad (1)$$

where $C_{m,i}$ and $C_{M,i}$ represent the concentration of Ion I in the micropores and macropores in the porous electrode, respectively; Z_i is species valence; V_T is the thermal voltage ($V_T=KT/e$, k and T are the Boltzmann constant and temperature, respectively, where T is usually set at 293.15K); $\Delta\phi_D$ is the Donnan potential; and $\overline{\mu}_{att}$ accounts for the non-electrostatic adsorption potential of ions into micropores.

The model assumes that the ion concentration in the macropore is electrically neutral (i.e. in the macropore, the double electric layer is ignored), that is,

$$\sum_i Z_i \cdot c_{M,i} = 0. \quad (2)$$

The charge density of the micro hole $\sigma_{m,i}$ is given by

$$\sigma_{m,i} = \sum_i Z_i \cdot C_{m,i}. \quad (3)$$

The charge density and potential drop $\Delta\phi_m$ in the microhole can be associated with the effective volume ratio capacitance C_m of the microhole, which is expressed as

$$\sigma_{m,i} \cdot \frac{F}{V_T} = -C_m \Delta\phi_m, \quad (4)$$

where $\sigma_{m,i}$ is the charge density in the micropore, F is the Faraday constant (96485 C·mol⁻¹), C_m is the effective volume-specific capacitance of micropores and $\Delta\phi_m$ is a micropore potential drop.

2.2.2 Transport model

Free and porous media flow fields are used to solve the velocity distribution and pressure distribution in the main channel and the porous electrode region. The fluid flow in the main channel satisfies the continuous Navier–Stokes momentum conservation equation [13] as follows:

$$\rho(\mathbf{u} \cdot \nabla)\mathbf{u} = \mu\nabla \cdot [\nabla\mathbf{u} + (\nabla\mathbf{u})^T] - \nabla p, \quad (5)$$

where ρ is the fluid density (kg·m⁻³), \mathbf{u} is the fluid velocity field vector (m·s⁻¹), p represents the internal pressure of the unit (Pa) and μ is hydrodynamic viscosity (Pa·s).

The fluid flow in the porous electrode region satisfies the continuous Stokes–Brinkman momentum conservation equation and conforms to Darcy's law [34] as follows:

$$\nabla \cdot (\rho\mathbf{u}) = S_i, \quad (6)$$

$$\left(\frac{\mu}{k} + S_i\right)\mathbf{u} = \frac{\mu}{\varepsilon_p} \nabla \cdot [\nabla\mathbf{u} + (\nabla\mathbf{u})^T] - \nabla p, \quad (7)$$

$$\mathbf{u} = -\frac{k}{\mu} \nabla p, \quad (8)$$

$$k = \varepsilon_p^3 / [\kappa A_s^2 (1 - \varepsilon_p)^2], \quad (9)$$

where S is the mass source term ($\text{kg}\cdot\text{m}^{-3}\cdot\text{s}^{-1}$, usually zero), ε_p is the porosity of the porous electrode, k is the porous electrode permeability, κ is the Kozeny–Carman constant [35] and A_s is the specific surface area of the porous electrode (m^{-1}).

The thin material transfer field is used to describe the transfer and concentration distribution of each group of isolates generated by convective diffusion in the unit. The electrostatic field is used to solve the distribution of electric potential in a cell by coupling these two fields. We have coupled the Nernst–Planck equation, which describes the mass transfer of all ions, and the Poisson equation, which describes the charge density and electric field.

According to the relationship between the change of electric potential and the surface charge density of the electrode, the CDI model conforms to the following Poisson equation:

$$\nabla \cdot (-\varepsilon_0 \varepsilon_r \nabla \phi) = \rho_C = F(c_+ - c_-), \quad (10)$$

where $\varepsilon_0 \varepsilon_r$ is the dielectric constant, ϕ is the local potential (V), ρ_C is the surface charge density of the electrode (C/m^2) and $c_+ - c_-$ is the difference in cation and cation concentration ($\text{mol}\cdot\text{m}^{-3}$).

The ion transport in the CDI model is described by the Nernst-Planck-Poisson equation, and the I ion flux J_i in the dilute NaCl solution is given by

$$J_i = -D_i \left(\nabla c_i + \frac{z_i F}{RT} c_i \nabla \phi \right) + u c_i, \quad (11)$$

where J_i is the ion mass flow diffusion vector ($\text{mol}\cdot\text{m}^{-2}\cdot\text{s}^{-1}$), D_i is the ion diffusion coefficient ($\text{m}^2\cdot\text{s}^{-1}$), c_i is the concentration of species i ($\text{mol}\cdot\text{m}^{-3}$), z_i is species valence, F is the Faraday constant ($96485 \text{ C}\cdot\text{mol}^{-1}$), R is the ideal gas constant ($8.314 \text{ J}\cdot\text{mol}^{-1}\cdot\text{K}^{-1}$) and T is the temperature in the cell (K).

Based on the original mass transfer formula (11) and the Bruggemann modified equation, the effective diffusion coefficient of the porous electrode region D_i^{eff} is modified as follows:

$$D_i^{\text{eff}} = \varepsilon_p^{3/2} D_i. \quad (12)$$

If no homogeneous ion reaction occurs in the solution, the conservation of mass of ions needs to be satisfied

$$\frac{\partial c_i}{\partial t} + \nabla \cdot J_i = R_i, \quad (13)$$

$$\nabla \cdot J_i = 0, \quad (14)$$

where R_i is the reaction rate density source term of I ion generation/removal. For electrolytes, this term is usually zero. In the area of porous electrode, due to the influence of porosity, the conservation of mass of ions also needs to be satisfied

$$\frac{\partial}{\partial t} \left(\varepsilon_p^{\text{eff}} c_i \right) + \nabla \cdot J_i = R_i. \quad (15)$$

2.3. Boundary conditions

(1) The inlet boundary condition is given by setting the inlet velocity as follows:

$$\mathbf{u} = \mathbf{u}_{in} = \mathbf{0}, \frac{0.025m}{s}. \quad (16)$$

(2) The exit boundary condition is given by setting the pressure outlet as follows:

$$\mathbf{p} = \mathbf{p}_{out} = \mathbf{0}. \quad (17)$$

(3) Electric field potential boundary condition

The positive electrode applies voltage, and the negative electrode is grounded:

$$\phi_+ - \phi_- = V_{cell} = 1.0V. \quad (18)$$

The Stern plane potential of the double electric layer ($x=\delta$) is ϕ_{Stern} , and the potential of the charged surface away from the electrode is zero, i.e.

$$\begin{cases} \phi(\delta) = \phi_{Stern} \\ \phi(\infty) = \phi_{bulk} = 0 \end{cases}. \quad (19)$$

3. RESULTS AND DISCUSSION

3.1. Model validation

According to the experimental process of CDI unit in reference [15] and the parameters set in the experiment (shown in Table 2 below), a complete adsorption and desorption cycle was calculated for the plate input–outflow CDI unit based on the MD model

Table 2. Experimental parameters of the CDI unit

Parameter	Unit	Value	Description
$c_{in,2}$	mol/m ³	20	Inlet concentration of NaCl solution
$u_{in,2}$	m/s	4.38×10^{-4}	Inlet flow rate of NaCl solution
V_2	V	1.0	electrode voltage

Figure 2 shows the comparison of the exit concentration normalisation (exit concentration/inlet concentration) curve of the NaCl solution calculated by a complete adsorption and desorption model in CDI unit with the experimental results. We adopt the dimensionless time parameters in figure \bar{t} ($\bar{t} = L_e^2/D_e$, L_e is the electrode thickness and D_e is the ion diffusion coefficient) to characterise the NaCl solution concentration of the export's relationship with time.

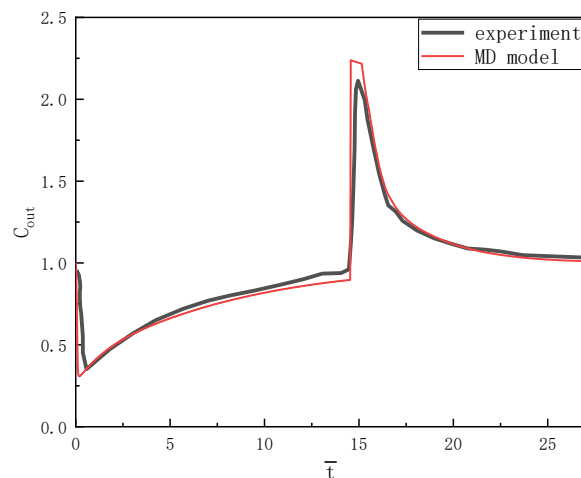
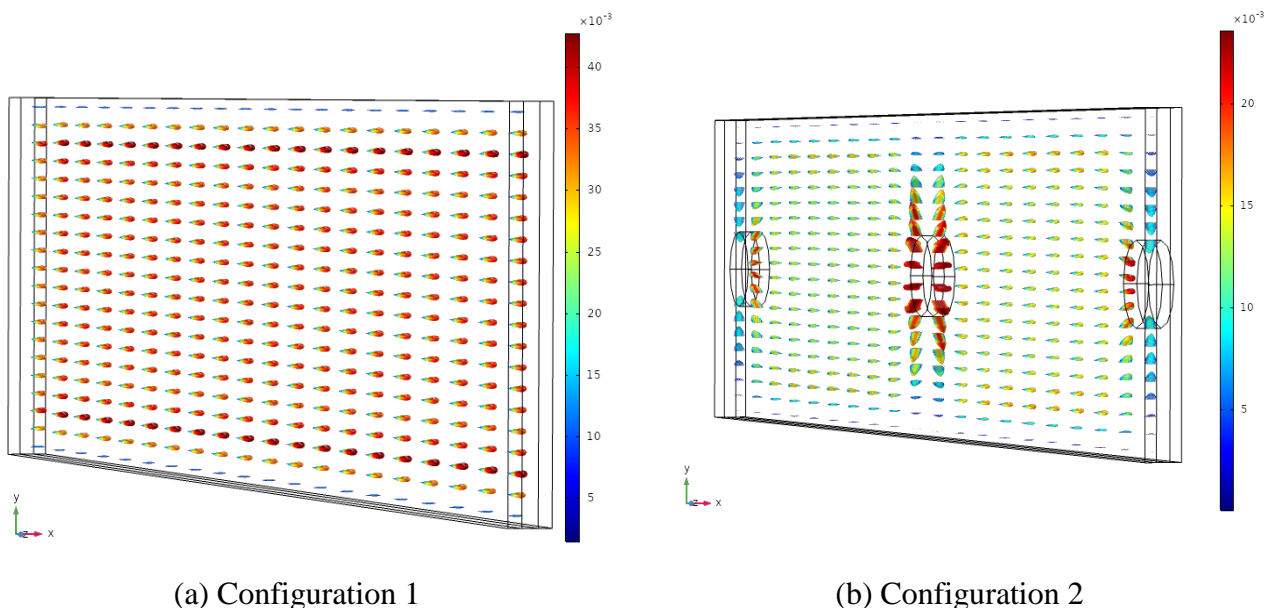


Figure 2. Comparison of the NaCl solution outlet concentration curve over time between the CDI experiment and model calculation

The calculation results in Figure 2 reveal that, in the CDI unit under $\bar{t} = 0 - 1$, the export concentration of the NaCl solution quickly reduced to the lowest point and then the export concentration rebounded. Furthermore, the rising rate gradually eased. The experimental results show that the same change rule is consistent; however, the rate of model export concentration decline is faster than the experimental data. This is because in the experiments, the preparation of activated carbon electrode is combined with activated carbon conductive agent and adhesive, mixed at a certain proportion and then daubed on the graphite plate [36], thus increasing the roughness of the electrode surface, which then affected the flow in the flow passage of the solution. The model does not take into account the actual situation under the influence of electrode surface roughness during the calculation, assuming that the electrode surface is smooth. Thus, the model solution flow is not affected by the surface of the electrode and the solution flows more smoothly. As shown in Figure 2, when $\bar{t} = 0 - 1$, the model concentration decline rate is faster than the experimental data.

3.2 Influence of different configurations of CDI cell on solution flow

The flow process of the NaCl solution in the channel of CDI cell under four configurations set in this paper was first calculated according to the parameters and boundary conditions given in Table 1. Figure 3 shows the flow field distribution inside the CDI cells with four configurations.



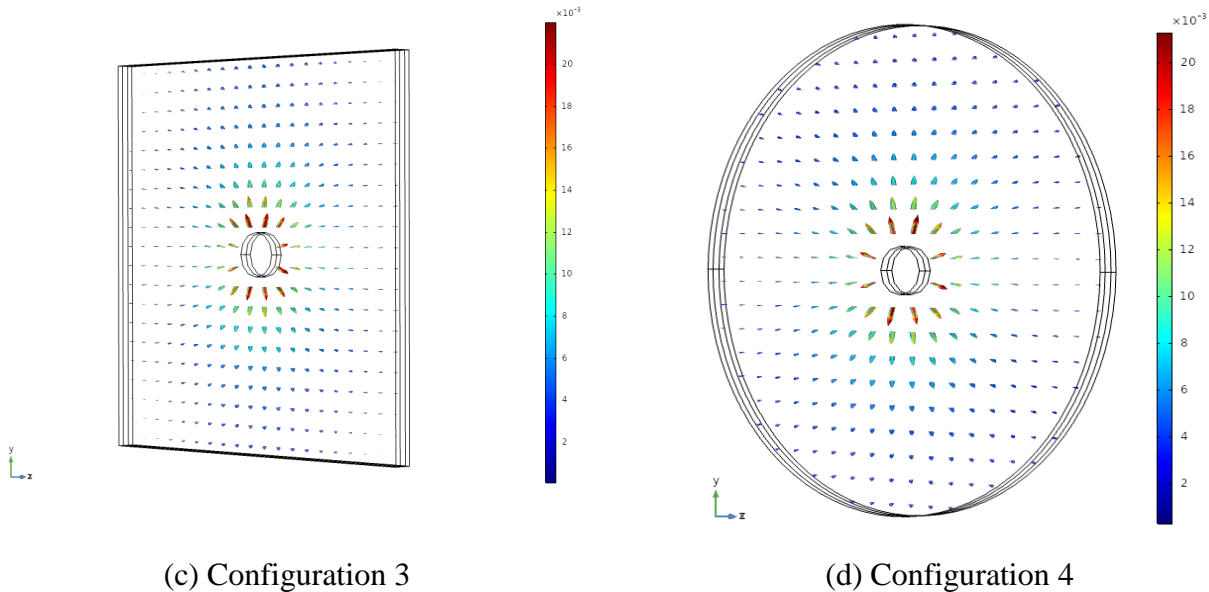


Figure 3. Solution flow distribution diagrams of CDI cell channels with different configurations

As shown in Figure 3, in Configuration 1, the flow passage velocity of the NaCl solution remained unchanged from the entrance to the exit. At the entrance to the Configuration 2 CDI unit, flow passage velocity is faster and decreased to 0.011797 m/s at the exit. In the four-corner unit, it can be seen that basic solution flow velocity is zero, and in the corner unit, the basic solution does not flow out.

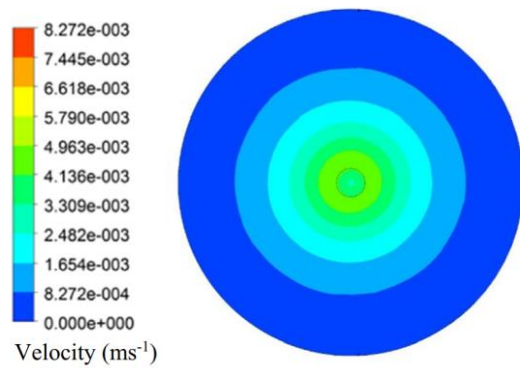


Figure 4. Fluent simulation solution flow diagram of the CDI unit with middle inflow and surrounding outflow

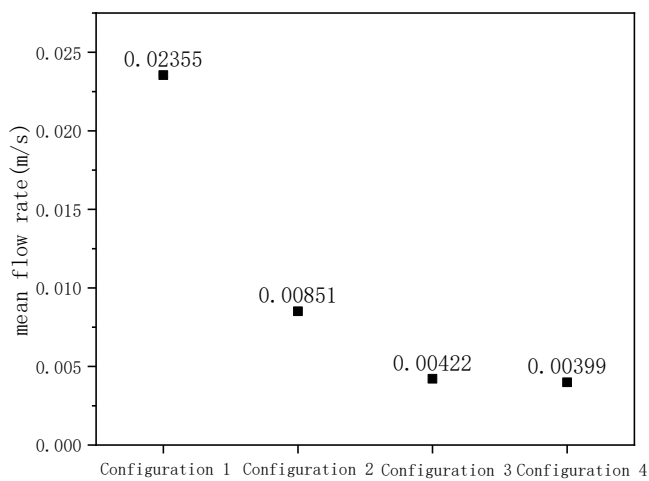


Figure 5. Average solution velocity diagram in the CDI cell channels in four configurations

Compared with the flow in the CDI unit 1 and unit 2 channels, when the NaCl solution flows in the CDI unit 3 and unit 4 channels, the velocity changes greatly at the inlet and decreases rapidly from 0.025 to 0.009316 and 0.009026 m/s, respectively. When the solution is far away from the inlet, the velocity decreases to 0.00084 and 0.000604 m/s at the outlet, respectively. Laxman [27] used Fluent software to establish a model for 4CDI configurational unit for simulation. The solution flow in the flow channel in that work is consistent with that shown in Figure 3(d). After the solution flowed in from the inlet, the flow velocity decreased rapidly. In addition, the flow velocity around the outlet was slowest, indicating that the model could correctly simulate the flow of solution in the flow channel. Furthermore, the 3CDI element and 4CDI elements can rapidly reduce the flow velocity of the solution in the flow passage at the inlet; thus, the flow velocity of the solution far away from the inlet was much lower than the inlet velocity at the initial moment.

The average flow velocity of NaCl solution in the flow channel of CDI cells in four configurations is shown in Figure 5. Notably, the average velocity of the NaCl solution in the flow channel was obtained by using the domain probe of COMSOL software. As shown in Figure 5, the average flow rates of the solutions in the channels of Configurations 1–4 were 0.0235, 0.00851, 0.00422 and 0.00399, respectively, indicating corresponding inlet flow rate reductions of 94.2%, 34.04%, 16.88% and 15.96%. The retention times of the solutions in the CDI cells of four configurations were 4.2, 5.88, 5.27 and 6.34 s, respectively, with the retention time in Configuration 1 being the shortest. Moreover, based on the CDI unit Configuration 1, the residence time of solution in the channel increased by 40%, 44.52% and 50.95% for the three other configurations, respectively. According to the simulation results in Figure 3 and the data shown in Figure 5, the average velocity of the solution in the flow channel can be effectively reduced and the residence time of the solution in the flow channel can be increased by modifying the configuration of the CDI cell, increasing the output points of the CDI cell and distributing the flow amongst multiple output points.

3.3 Influence of different configurations of CDI cells on desalination capacity

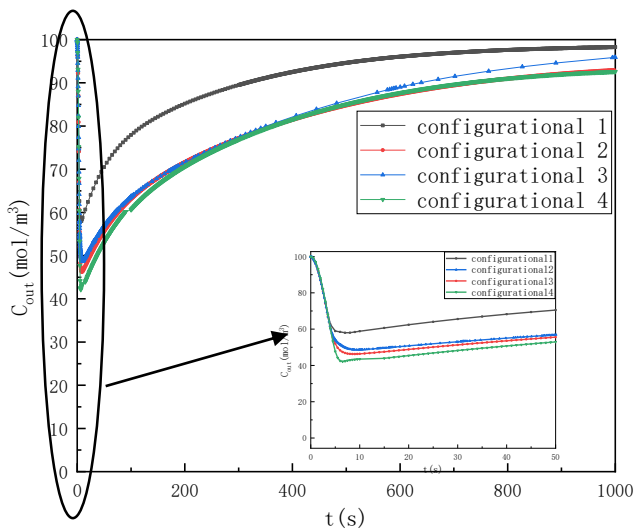


Figure 6. Outlet concentration diagram of different configurations in the adsorption stage

According to the parameters and boundary conditions given in Table 1, the adsorption process of CDI cells in four configurations was calculated. Figure 6 shows the comparison curves of the NaCl solution outlet concentrations under the same boundary conditions (the average value of the NaCl solution at the outlet boundary was obtained using the boundary probe of COMSOL software).

As shown in Figure 6, the NaCl solution outlet concentrations of CDI units in four configurations changed in the same way with time (i.e. rapidly decreasing to the lowest point first and then slowly increasing), although the rate of increase gradually slowed down. The adsorption performances of four types of CDI cells increased step by step; the CDI cell of Configuration 4 had the best adsorption performance. Combined with the analysis in Figure 5, we can assume that this was mainly caused by the different flow rates of the solution in the runner.

The outlet concentration curves of the CDI elements of Configurations 3 and 4 were relatively close. Firstly, because of their similar configuration, both of them flowed into the middle and flowed out onto the surrounding areas. Secondly, the average flow velocities of the solutions in the two channels showed slight variations, but both were slower than the first two configurations. However, the residence time of the solution in the flow channel of Configuration 4 CDI cell was longer than that of Configuration 3 CDI cell; thus, the NaCl solution outlet concentration of Configuration 4 CDI cell was lower than that of Configuration 3 CDI cell.

In order to better compare the adsorption capacities and maximum adsorption points selected (phase adsorption initial concentration of NaCl solution exports reached its lowest point in time) for the observation points in time amongst the four configurations of CDI units, we intercepted the YZ plane $X = 0.9, 1.1, 1.3$ mm in the solution of Cl^- concentration distribution, as shown in Figure 7. Then, we observed the CDI unit flow passage of the solution of Cl^- distribution in all four configurations.

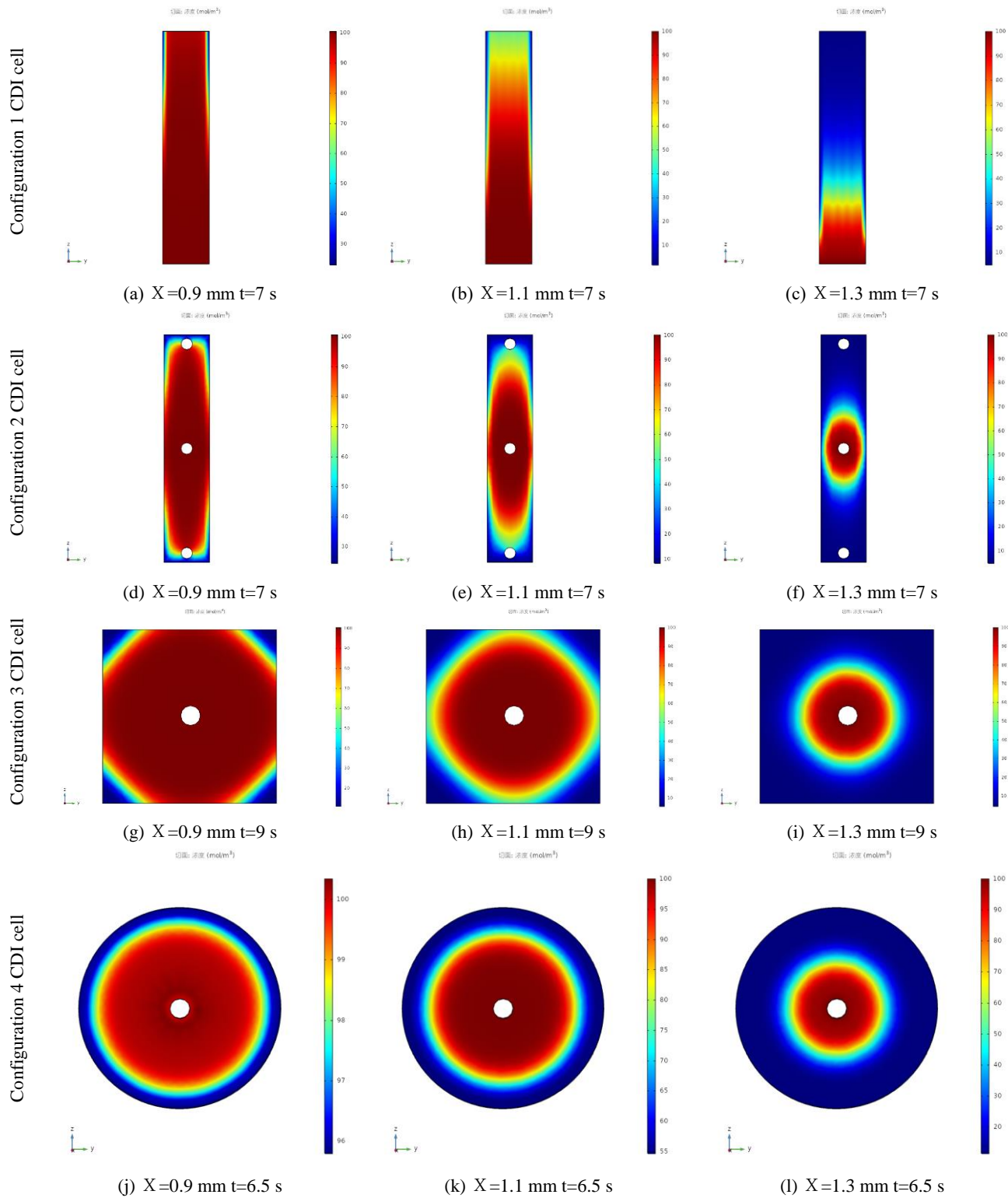


Figure 7. Cl^- -concentration distribution diagrams of channel YZ cross-sections of the CDI cells with different configurations

As shown in Figure 7, in the CDI unit flow passages, the effect of electric field force can be seen near the negative electrode on one side (Cl^- journeyed positive electrode side), resulting in the very low negative electrode on one side of the Cl^- concentration. The farther the positive electrode side, the higher

the concentration of Cl^- . Given that the solution flow rate was faster within the Configuration 1 CDI unit, the migration of Cl^- to the surface of the electrode had not fully passed the adsorption storage in the electric double layer. This allowed the solution to flow out of the CDI unit. Thus, in Configuration 1 CDI unit, Cl^- concentration was high near the positive electrode side exit.

Meanwhile, the flow rate of the solution in the channel of the CDI unit in Configuration 2 was close to zero in the four corner regions, so the residence time was longer. This meant that the Cl^- has sufficient time to migrate to the electrode surface and be absorbed and stored in the double electric layer. Therefore, the concentration of Cl in the side near the positive electrode was very low in the four corners. Furthermore, the concentration of Cl in the solution of the Configuration 3 CDI unit and Configuration 4 CDI unit was the same on the side close to the negative electrode. The concentration of Cl^- in the solution was high at the entrance, before significantly decreasing to less than 30 mol/m^3 at 12 mm away from the entrance. This indicated that, with the decrease of the flow rate of the solution, the Cl in the solution moved to the side of the positive electrode under the drive of the electric field force. On the side near the positive electrode, the concentration of Cl^- in the solution of the Configuration 3 CDI unit was very low at the four corners of the outlet, whilst the concentration of Cl^- in other regions was slightly higher. The concentration of Cl^- in Configuration 4 CDI elements was very low and evenly distributed at the exit, which greatly differed from that in Configuration 3. Combined with the analysis in Figure 3, this can be attributed to the different inlet to outlet path lengths in the three CDI unit configurations, which results in the different velocity directions of the solution and durations of flow passage.

In addition, the export of the four corner velocity solution in Configuration 3 was slower and residence time was longer than in other areas. Thus, the Cl^- concentrations from the inlet to outlet flowing onto the four corners had plenty of time under the action of electric field force. As a result, the Cl^- migrated to the surface of electrode and other areas because the entrance to the exit export path was shorter. Meanwhile, the concentration of Cl^- in the solution at the exit of Configuration 3 was uneven, with low concentration in the four corners and high concentration in other areas. At the same time, the distance of Configuration 4 was consistent from the inlet to the outlet in each direction; thus, the residence time of the solution in the electrode was also consistent. As a result, the concentration of Cl at the outlet of Configuration 4 was uniform: low on the side close to the positive electrode.

By comparing the adsorption capacity of CDI cells with different configurations conducted by Laxman[27], it can be seen that the fluid distribution type in CDI cells has a significant influence on the overall desalination performance. When the configuration design of CDI cell is not reasonable, such as configuration 2, in the desalination process, there is a large dead zone at the corner of the flow channel, which reduces the utilization rate of the electrode. Therefore, configuration 3 and 4 are more reasonable.

3.4 Influence of different configurations of CDI cells on desalination capacities at varying inlet flow rates

With other condition parameters unchanged in Table 1, the comparison curves of the average concentration of NaCl solutions at the exits of four types of CDI units during the adsorption process under different inlet flow rates (0.015, 0.02, 0.025, 0.03 and 0.035 m/s) are shown in Figure 8

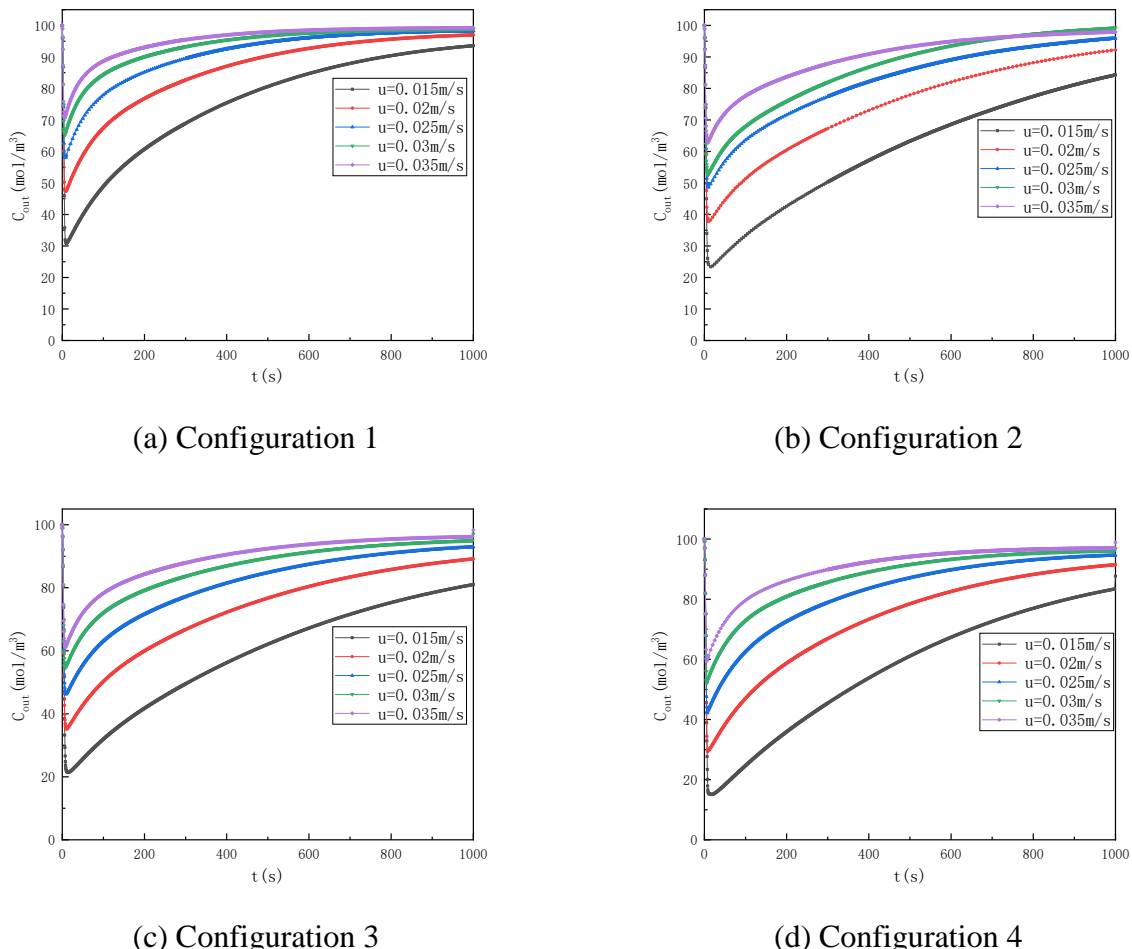


Figure 8. Outlet concentration curves of the NaCl solutions in CDI units in four configurations at different inlet flow rates

As shown in Figure 8, with the increase of inlet velocity, a higher concentration led to exports showing increasing inlet velocity and decreased desalination performance of the CDI unit. This is because the increase of solution inlet velocity induces the solution to stay in the flow passage at a shorter time. As a result, the ions migrating to the surface of electrode were not fully stored in the electric double layer adsorption, thus allowing the outflow of the solution and reducing the electrode adsorption capacity. By comparing and analyzing the experimental results of Hemmatifar[15], it was found that when the inlet flow rate decreased, the better the desalination effect was, and the lowest point of outlet concentration was lower. However, the moment when the lowest point of outlet concentration reached was basically the same, indicating that the curve of outlet concentration under different inlet flow rates of this model was consistent with the actual situation. As shown in Figure 9, the inlet velocity changed from 0.035 to 0.025 m/s, indicating small variations in the export concentration of the NaCl solution. In comparison, when the inlet velocity changed from 0.025 to 0.015 m/s, this indicated large variations in the export concentrations of the NaCl solutions. In practical applications, when the flow velocity is too small, the residence time of the solution in the flow passage increases greatly. The solution staying in

the flow passage reduces the water purification per unit time, which in turn, lowers the efficiency of the CDI process.

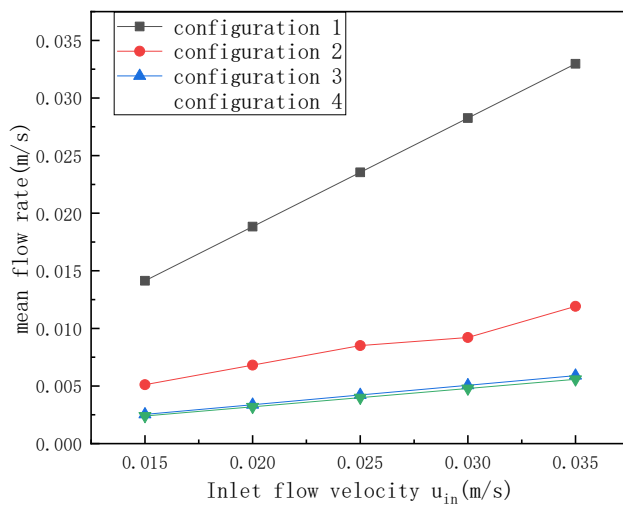


Figure 9. Average flow velocity diagram of CDI unit solutions under four configurations at different inlet flow rates

As shown in Figure 9, the average flow velocity of the solution in the flow channel of the CDI cells in four configurations had a linear relationship with inlet velocity. In particular, for every 0.005 m/s increase in inlet velocity, the average flow velocity of the solution of Configuration 1 increased by 0.0047 m/s. The average flow velocities of solutions in Configurations 2, 3, and 4 increased by 0.00169, 0.0008425 and 0.0008 m/s, respectively. This indicates that Configurations 3 and 4 can effectively reduce the influence of increasing inlet flow velocity on the average flow velocity of the solutions in the CDI unit channels.

4. CONCLUSIONS

In this paper, we established an MD model that considers the solution flow of charge transport electric potential and electric field coupling capacitance to examine the ion water desalination units of three dimensional transient models. The experimental data of Hemmatifar [15] were used to prove that the model could accurately describe the seawater desalination process of CDI units with porous carbon electrodes. By comparing the simulation results of CDI units with the inflow in the middle and outflow around the disk with those presented by Laxman [27], we were able to prove that the proposed 3D transient model can accurately simulate the flow of solution in the channel. Further, we used CDI units with four different configurations and the flow of the solutions to study the influence of ion adsorption and inlet velocities on the desalination performance of the four CDI units. The following conclusions are drawn:

- 1) At the entrance velocity and plate electrode area of certain cases, the CDI unit desalination capacity under the influence of the voltage and solution flow can effectively reduce the average flow

velocity of the solution and flow passage of time, thus improving the desalting ability of the CDI unit. This can be achieved by increasing the CDI unit output quantity and reducing the electrode component flow path from the entrance to the outlet through the CDI units.

2) Compared with the other three types of CDI units, the flow rate of the solution at four corners tends to be 0 m/s when the mid-hole flows into the open-hole outflow CDI unit at both ends of the plates. This prevents the solution from flowing out, thus weakening the desalination performance of the CDI unit.

3) Under the same boundary conditions, the desalination capacity of CDI cells decreases with the increase of inlet flow rate. The influence of the increase of inlet flow rate on the desalination performance of CDI cells can be reduced by increasing the number of output points.

References

1. J.M. Gozámez, J. Lora, J.A. Mendoza, M. Sancho, *Desalination*, 144(2002)341.
2. S. Porada, R. Zhao, A.V.D. Wal, V. Presser, P.M. Biesheuvel, *Prog. Mater Sci.*, 58(2013) 1388.
3. M. E. Suss, S. Porada, X. Sun, P.M. Biesheuvel, J. Yoon, V. Presser. *Energy Environ. Sci.*, 8 (2015) 2296.
4. J. -B. Lee; K. -K. Park, H. -M. Eum, C. -W. Lee, *Desalination.*, 196(2006)125.
5. P. Dlugolecki, A. Wal, *Environ. Sci. Technol.*, 47(2013).
6. H. Amy, D. Rice, University, (2015)
7. R. Zhao, P. M. Biesheuvel, H. Miedema, H. Bruning, A.V.D. Wal, *Phys. Chem. Lett.*, (2010).
8. P.M. Biesheuvel, Y. Fu, M. Z. Bazant, *J. Russ. Electrochim.*, 48(2012)580.
9. R. Zhao, P.M. Biesheuvel, A. V. D. Wal, *Energy Environ. Sci.*, 5(2012)9520.
10. R. Zhao, M.V. Soestbergen, H.H.M. Rijnaarts, A.V.D. Wal, M.Z. Bazant, P.M. Biesheuvel, *Colloid, Interface Sci.*, 384(2012)38.
11. S. Porada, M. Bryjak, A.V.D. Wal, P.M. Biesheuvel, *Electrochim. Acta*, 75(2012)148.
12. K. Kamran, M.V. Soestbergen, L. Pel, *Transp. Porous Media*, 96(2013)221.
13. P.M. Biesheuvel, Y. Fu, M.Z. Bazant, *J. Russ. Electrochim.*, 48(2012)580.
14. M.E Suss, T.F. Baumann, W.L. Bourcier, C.M. Spadaccini, K.A. Rose, J.G. Santiago, M. Stadermann, *Energy Environ. Sci.*, 5(2012)9511.
15. A. Hemmatifar, M. Stadermann, J.G. Santiago, *Phys. Chem. C*, (2015).
16. F. He, P.M. Biesheuvel, M.Z. Bazant, T. Alan Hatton, *Water Res.*, 132 (2018)282.
17. E.N. Guyes, A.N. Shocron, A. Simanovski, P.M. Biesheuvel, M.E. Suss, *Desalination*, 415(2017)8.
18. Y.A.C. Jande, W.S. Kim, *Sep. Purif. Technol.*, 115(2013)224.
19. Z.L. Chen, H.T. Zhang, C.X. Wu, L.T. Luo, C.P. Wang, S.B. Huang, H. Xu, *Desalination*, 433(2018)68.
20. Y. Li, Y.X. Liu, J.M. Shen, J.W. Qi, J.S. Li, X.Y. Sun, J.Y. Shen, W.Q. Han, L.J. Wang, *Desalination*, 430(2018)45.
21. K. Laxman, M.T.Z. Myint, R. Khan, T. Pervez, J. Dutta, *Electrochimica Acta*, 166(2015)329.
22. M.W. Saleem, W.-S. Kim, *Desalination*, 437(2018)133.
23. E.M. Remillard, A.N. Shocron, J. Rahill, M.E. Suss, C.D. Vecitis, *Desalination*, 444(2018)169.
24. K. Laxman, L.A. Gharibi, J. Dutta, *Electrochim. Acta*, 176(2015)420.
25. E.N. Guyes, A. Simanovski, M.E. Suss, *RSC Adv.*, 7(2017)21308.
26. Y.S. Jeon, S.I. Cheong, J.W. Rhim, *Macromol. Res.*, 25(2017)712.
27. K. Laxman, A. Husain, A. Nasser, M.A. Abri, J. Dutta, *Desalination*, 449(2019)111.
28. E.N. Guyes, A.N. Shocron, A. Simanovski. P.M. Biesheuvel, M.E. Suss, *Desalination*, 415(2017)8.

29. H.K. Mutha, H.J. Cho, M. Hashempour, B.L. Wardle, C.V. Thompson, E.N. Wang, *Desalination*, 437(2018)154.
30. S.G. Yao, J.W. Wu, *Desalin. Water Treat.*, 144(2019)1.
31. M.E. Suss, P.M. Biesheuvel, T.F. Baumann, M. Stadermann, J.G. Santiago, *Environ. Sci. Technol.*, 48(2014)2008.
32. P.M. Biesheuvel, Y.Q. Fu, M.Z. Bazant, *Phys. Rev. E*, 83(2011)61507.
33. P.M. Biesheuvel, S.Porada, M. Levi, M.Z. Bazant, *Solid State Electrochem.* 18(2014)1365.
34. A. Jemni, S.B. Nasrallah, *Int. J. Hydrogen Energy*, 20(1995)881.
35. A. Mhimid. *Int. J. Heat Mass Transfer*, 41(1998)2967.
36. X.J. Yao, Y.G. Cai, M.Y. Guo, K.J. Bao, Z.Sun, Y.N. Ye, X.Q.Piao, *Micronanoelectronic Technology*, 57(2020)270.

© 2021 The Authors. Published by ESG (www.electrochemsci.org). This article is an open access article distributed under the terms and conditions of the Creative Commons Attribution license (<http://creativecommons.org/licenses/by/4.0/>).